삼중 루우프 제어방식을 채택한 분산형 전력시스템을 위한 멀티 모듈 승압형 컨버터

최 병 조 한 동 훈
경북대학교 전자전기공학부

A Multi-Module Three-Loop Controlled Boost Converter for Distributed Power Applications

Byungcho Choi Donghoon Han
School of Electronic and Electrical Engineering
Kyungpook National University

Abstract--This paper presents the control design of a three-module boost converter with a two-stage output filter. An advanced three-loop control scheme is employed to the control design in order to obtain good dynamic performance of the converter at the presence of the secondary filter stage. The paper presents the control design, dynamic analysis and performance improvement with the three-loop control.

1. Introduction

Multi-module boost converters are being widely used as battery dischargers [1,2] in space power systems and telecommunication power supplies with battery back-up. For those applications, a two-stage output filter [1,3] is frequently used to reduce the ripple at the output voltage of the boost converter. Despite its associate benefits, however, the use of the two-stage filter presents a challenge to designing the control loop of the converter. The secondary stage of the two-stage filter introduces an additional resonance, and severely deteriorates the phase characteristics of the duty cycle-to-output transfer function. For satisfactory performance of the converter, the secondary filter resonance should be adequately controlled by the feedback compensation. However, the conventional two-loop current mode control does not offer any means of controlling the secondary filter resonance, and design attempts using the two-loop control would result in poor performance.

An earlier work [4] proposed a three-loop control which could nullify the detrimental effects of the secondary filter resonance. The three-loop control in its original form was developed for buck-derived topologies, and has not been extended to any other topologies. This paper presents the three-loop control of a three-module boost converter with a two-stage output filter. The paper demonstrates that the three-loop control scheme, initially aimed for buck-derived topologies, can be adapted to the boost converter, offering a significant improvement in performance. The paper presents the details about the three-loop control and performance enhancement with the advanced control scheme.

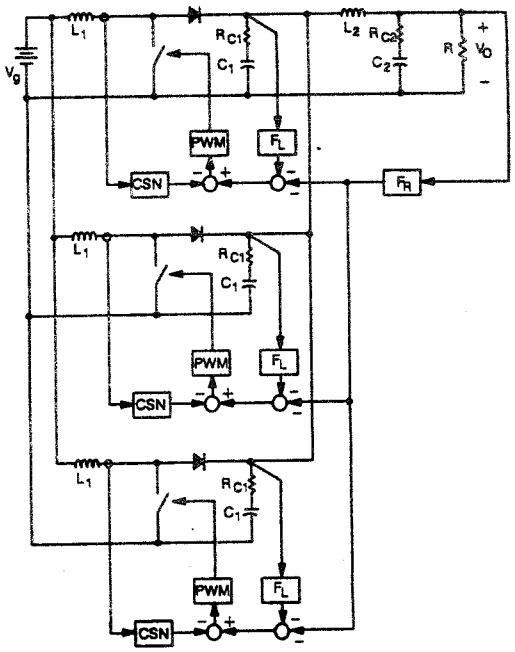

Fig. 1. Three-module boost converter with a two-stage output filter: $V_g = 24V$, $V_o = 50V$, $R = 10\Omega$,

2. Three-Module Boost Converter

Figure 1 shows the three-module boost converter with the three-loop control. The converter consists of three boost modules, a secondary LC filter (L_2, and C_2), and an output voltage feedback circuit F_R. Each module consists of a boost power stage, a pulse width modulation (PWM) block, a current sensing network (CSN) for inductor current feedback, and an additional feedback circuit F_L for the voltage feedback from its output capacitor. This inner voltage feedback is defined as the "local voltage feedback," and the voltage feedback from the output will be referred to as the "remote voltage feedback." When the local voltage feedback is removed ($F_L = 0$), the three-loop control reduces to the conventional two-loop current mode control.

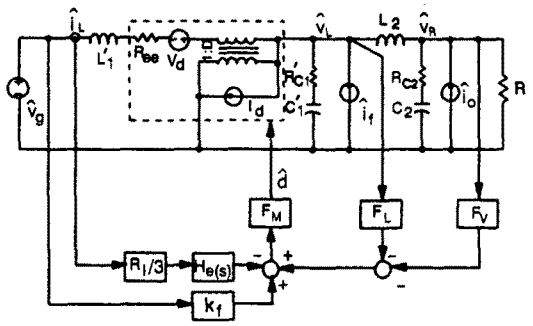

Fig. 2. Reduced-order small-signal model of the three-module converter: F_M represents the modulator gain of the PWM block, and R_i is the dc gain of CSN of individual module.

3. Principles of Three-Loop Control

A. Open-Loop Analysis

Figure 2 shows the reduced-order small-signal model of the converter [4]. The model has the structure of a single-module converter, yet retains the small-signal dynamics of the original three-module converter. The transfer functions from the duty cycle to various feedback signals can be derived from Fig. 2:

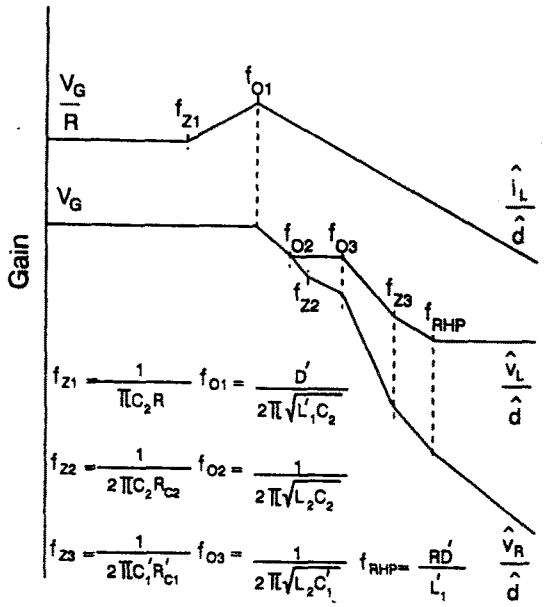

Fig. 3. Power stage transfer functions.

$$\frac{\hat{v}_R}{\hat{d}} \cong \frac{V_g}{D'^2} \frac{\left[1+sC_1'R_{C1}'\right]\left[1+sC_2R_{C2}\right]\left[1-sL_1'/D'^2R\right]}{\left[1+s\left(C_2(R_{C2}+R_{C1}'D/D')+L_1'/D'^2R\right)+s^2L_1'C_2/D'^2\right]\left[1+sC_1'(R_{C1}'+R_{C2})+s^2L_2C_1'\right]} \tag{1}$$

$$\frac{\hat{v}_L}{\hat{d}} \cong \frac{V_g}{D'^2} \frac{\left[1+sC_1'R_{C1}'\right]\left[1+s(L_2/R+C_2R_{C2})+s^2L_2C_2\right]\left[1-sL_1'/D'^2R\right]}{\left[1+s\left(C_2(R_{C2}+R_{C1}'D/D')+L_1'/D'^2R\right)+s^2L_1'C_2/D'^2\right]\left[1+sC_1'(R_{C1}'+R_{C2})+s^2L_2C_1'\right]} \tag{2}$$

$$\frac{\hat{i}_L}{\hat{d}} \cong \frac{2V_O}{D'^2R} \frac{\left[1+sC_2R/2\right]}{\left[1+s\left(C_2(R_{C2}+R_{C1}'D/D')+L_1'/D'^2R\right)+s^2L_1'C_2/D'^2\right]} \tag{3}$$

with assumptions $L_1' >> L_2$, $C_2 >> C_1'$, $R >> R_{C1}'$, $R >> R_{C2}$, $C_1'R_{C1}' >> L_2/R$, and $C_1'R_{C2} >> L_2/R$.

Figure 3 shows the asymptotic plots for the transfer functions of (1), (2), and (3). The secondary filter resonance between L_2 and $C_1'(f_{O3})$ is apparent in both $\hat{v}_R/\hat{d}$ and $\hat{v}_L/\hat{d}$. This secondary resonance causes -180° phase delay to the phase of $\hat{v}_R/\hat{d}$, presenting a substantial problem to the two-loop control [4]. The basic idea of the three-loop control is to use $\hat{v}_L/\hat{d}$ as an integral part of the controller. This in effect erases the impacts of the secondary filter resonance, thereby eliminating the problems found in the two-loop control. As shown in Fig. 3, the RHP zero, $f_{ESR} = RD'^2/2\pi L_1'$, is placed at high frequencies by an appropriate selection of the power stage parameters. Pushing the RHP zero toward high frequencies not only minimizes adverse effects of the RHP zero but also maximizes the advantage of the local voltage feedback. If the RHP zero is placed at lower frequencies, the effects of the local voltage feedback would be limited.

B. Three-Loop Control

Figure 4 illustrates the principles of the three-loop control in comparison with a two-loop control. The current loop T_I, local loop T_L, and the remote loop T_R represent the individual gain of the control loop associated with the corresponding feedback signal. The asymptotic plots of individual feedback loops are obtained by combining the power stage transfer functions of the Fig. 3 and feedback compensations shown in Table I. For the three-loop control, the remote loop is dominant at low frequencies, and the current loop is dominant at high frequencies, as is the case for two-loop control. In the mid-frequency region, however, the local loop is designed to prevail over the remote and the current loops. The dominance of the local voltage loop at the mid-band offers: 1) an absorption of the secondary filter resonance into the feedback loop, thereby minimizing the adverse effects of the secondary resonance, and 2) a gain boost in the mid-band, improving the frequency-domain performance.

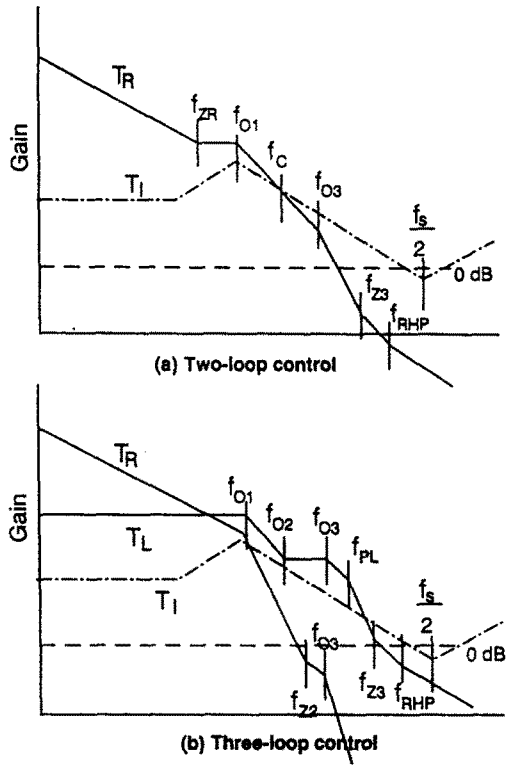

Fig. 4. Comparison of control schemes.

4. Performance Enhancement with Three-Loop Control

For an informative assessment of the three-loop control, the performance of the three-loop controlled converter is compared with that of the two-loop controlled converter. Compensation parameters used in this comparative analysis are shown in Table I.

A. Frequency-Domain Performance

Figure 5(a) compares the overall loop gain[4] measured at the output of the PWM block, and Fig. 5(b) shows the outer loop gain[4] measured at the output of the voltage feedback compensation. Compensation parameters are chosen such that two converters with different control schemes result in the same high-frequency characteristics of the overall loop gain, and the same phase margin of the outer loop gain. The loop gains indicate that both cases are designed in an optimal manner, yet maintain 60° phase margin in the outer loop gain.

The audio-susceptibility, $\hat{v}_R / \hat{v}_g$ (Fig. 5. (c)), and the output impedance, $\hat{v}_R / \hat{i}_o$ (Fig. 5. (d)), show improvements with the three-loop control; the low-frequency gain is reduced, and the peaking at the secondary resonance is removed. This would improve the speed and transient

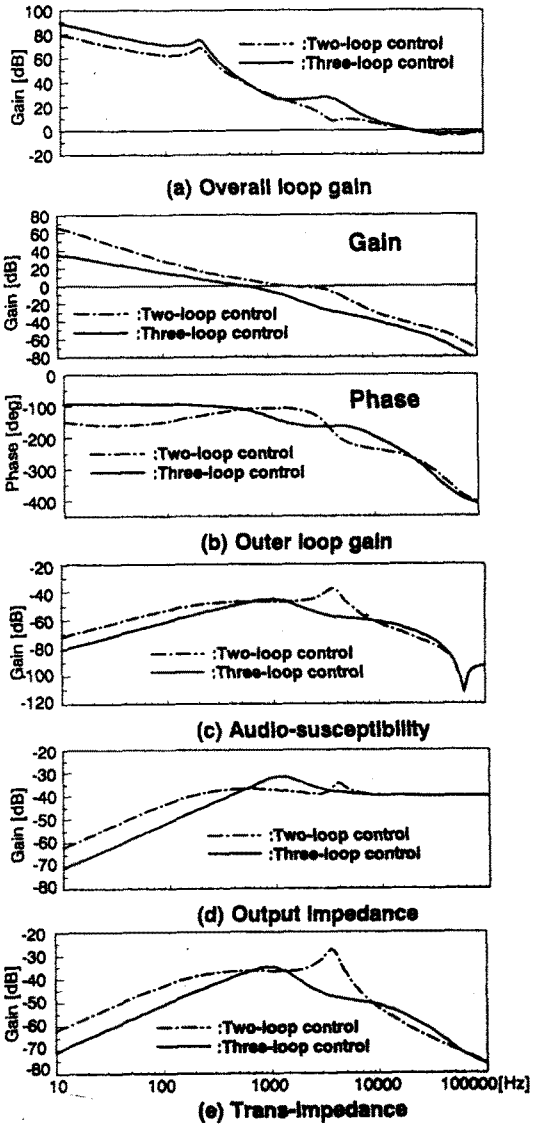

Fig. 5. Frequency-domain performance.

behavior of the time-domain performance. Figure 5(e) compares the trans-impedance, $\hat{v}_O / \hat{i}_f$, which could characterize the transient response of the output voltage in the event of the failure of an individual module. The improvement similar to the case of the audio-susceptibility can be also observed in Fig. 5 (e).

B. Time-Domain Performance

Transient responses of the output voltage due to the step input change (Fig. 6 (a)), due to the step load change (Fig. 6(b)), and due to the switch-open failure of the third module (Fig. 6(c)) are compared in Fig. 6. The three-loop controlled converter shows faster, better-damped transient behavior of the output voltage with reduced overshoot/undershoot.

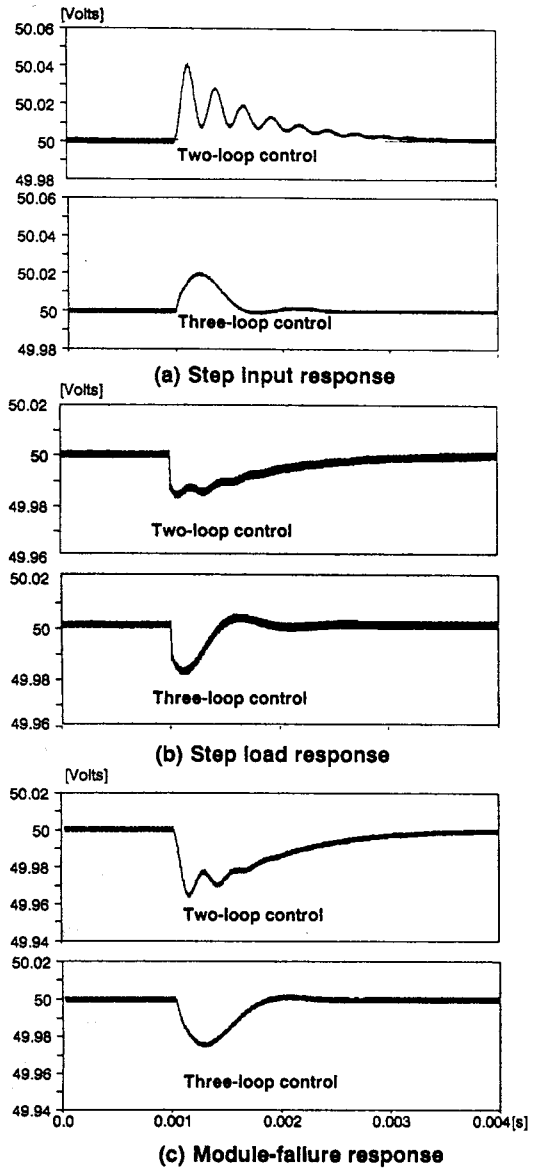

Fig. 6. Time-domain performance: (a) Transient response of the output voltage when the input voltage changes from *24 Volts* to *30 Volts*; (b) When the load resistor changes from $10\,\Omega$ to $8\,\Omega$; (c) When the switch of the third module remains open at *1 msec*.

5. Effects of Location of the RHP Zero on the Closed -loop Performance

As shown in Fig. 3, the RHP zero is located at high frequencies in order to maximize the benefits of the local voltage feedback. Otherwise, the effects of the local voltage feedback will be limited. Figure 7 shows the performance comparison when $f_{O3} < f_{RHP} < f_{Z2}$. As shown in the Fig. 7, the performance improvement is not as significant as that of the previous case.

6. Conclusions

The three-loop control scheme, originally developed for buck-derived topologies, has been successfully adapted to a three-module boost converter with two-stage output filter. The three-loop control is most effective if the power stage parameters are chosen to push the RHP zero of transfer functions to high frequencies. A significant improvement in closed-loop performance, particularly the transient response in the event of failure of an individual module, has been achieved with the three-loop control scheme.

The superiority of the three-loop control over the conventional two-loop control has been verified by both frequency- and time-domain simulations.

References

[1] D. M. Sable, and R.B. Ridley, " A high-frequency multi-module, spacecraft boost regulator," VPEC Power Electronic Seminar, 1998 Record, pp. 178-186.

[2] D. M. Sable, S. Deuty, F.C. Lee, and B.H. Cho, " Experimental verification of space platform battery discharger design optimization," Intersociety Energy Conversion Engineering Conference, 1991 Record.

[3] R.B. Ridley, "Secondary LC filter analysis and design techniques for current-mode-controlled converters," IEEE Trans. Power Electron., vol. 3, pp.499-507, Oct. 1988.

[4] B. Choi, B. H. Cho, F.C. Lee, and R.B. Ridley, "Three-loop control for multi-module converter systems," IEEE Trans. Power Electron., vol. 8, pp. 466-474, Oct. 1993.

[5] R.B. Ridley, "A new continuous-time model for current-mode control," IEEE Trans. Power Electron., vol. 6, pp. 271-280, Apr. 1991.

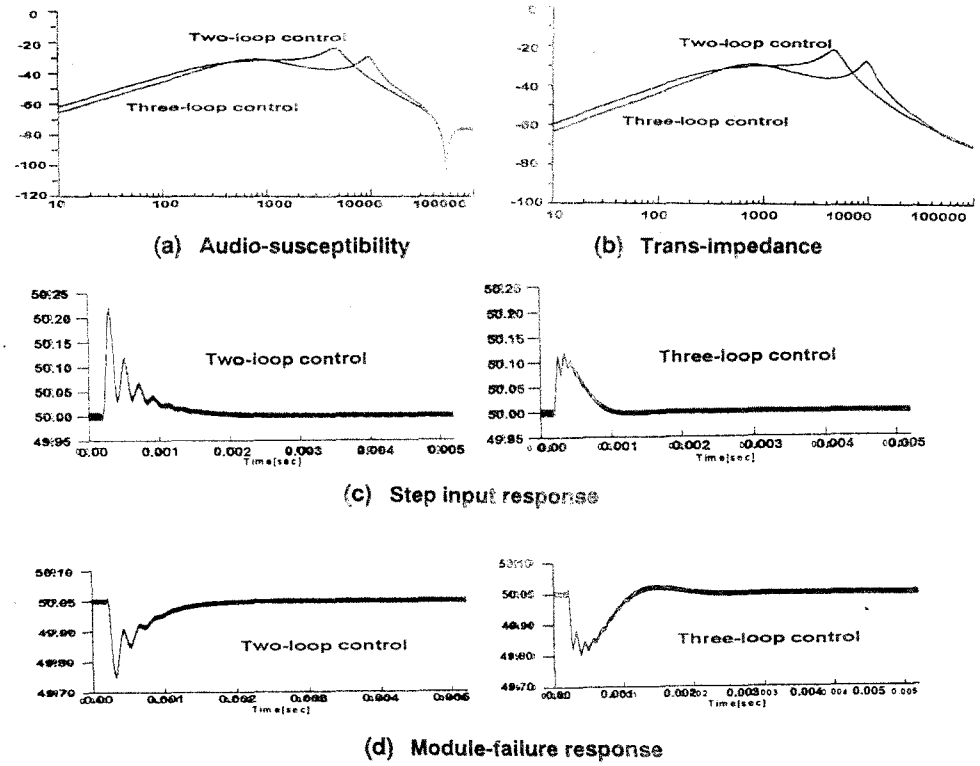

Fig. 7. Closed-loop performance: (a) Audio-susceptibility; (b) Trans-impedance; (c) Transient response of the output voltage when the input voltage changes from *24 Volts* to *30 Volts*; (d) When the switch of the third module remains open at *1 msec*.

Table I: Summary of Compensation Parameters

	Two-loop control	Three-loop control
Feedback Compensation Parameters	$F_R(s)=\frac{K_R(1+s/\omega_{ZR})}{s(1+s/\omega_{PR})}$ $K_R = 38600$, $\omega_{ZR}=0.8/\sqrt{L_1C_2}=1107[r/s]$ $\omega_{PR}=1/C_1R'_{C1}=13251[r/s]$ $F_L(s)=0$	$F_R(s)=\frac{K_R}{s}$ $K_R = 110050$, $F_L(s)=\frac{K_L}{(1+s/\omega_{PL})}$ $K_L = 35[r/s]$ $\omega_{PR}=1.2/\sqrt{L_2C_1}=26400[r/s]$
For both two-loop and three-loop control: $R_i = 0.2353$, $F_M = 0.1454$, $k_f = -0.084$ $H_e(s)=1+s/\omega Q+s^2/\omega^2$, $Q=-2/\pi$, $\omega=\pi\times10^5$		